9848 *Biochemistry* **2009,** *48,* 9848–9857
DOI: 10.1021/bi901126u

BIOCHEMISTRY
including biophysical chemistry & molecular biology
Article

Effects of pH on the Rieske Protein from *Thermus thermophilus*: A Spectroscopic and Structural Analysis[†,‡]

Mary E. Konkle,[§] Sarah K. Muellner,[§] Anika L. Schwander,[§] Michelle M. Dicus,[∥] Ravi Pokhrel,[§,⊥] R. David Britt,[∥] Alexander B. Taylor,[#] and Laura M. Hunsicker-Wang*[,§]

[§]*Department of Chemistry, Trinity University, One Trinity Place, San Antonio, Texas 78212,* [∥]*Department of Chemistry, University of California at Davis, One Shields Avenue, Davis, California 95616, and* [#]*Department of Biochemistry and X-ray Crystallography Core Laboratory, University of Texas Health Science Center at San Antonio, San Antonio, Texas 78229* [⊥]*Current address: Department of Chemistry, Yale University, 225 Prospect St., New Haven, CT 06520*

Received July 2, 2009; Revised Manuscript Received September 2, 2009

ABSTRACT: The Rieske protein from *Thermus thermophilus* (*Tt*Rp) and a truncated version of the protein (trunc*Tt*Rp), produced to achieve a low-pH crystallization condition, have been characterized using UV−visible and circular dichroism spectroscopies. *Tt*Rp and trunc*Tt*Rp undergo a change in the UV−visible spectra with increasing pH. The LMCT band at 458 nm shifts to 436 nm and increases in intensity. The increase at 436 nm versus pH can be fit using the sum of two Henderson−Hasselbalch equations, yielding two pK_a values for the oxidized protein. For *Tt*Rp, pK_{ox1} = 7.48 ± 0.12 and pK_{ox2} = 10.07 ± 0.17. For trunc*Tt*Rp, pK_{ox1} = 7.87 ± 0.17 and pK_{ox2} = 9.84 ± 0.42. The shift to shorter wavelength and the increase in intensity for the LMCT band with increasing pH are consistent with deprotonation of the histidine ligands. A pH titration of trunc*Tt*Rp monitored by circular dichroism also showed pH-dependent changes at 315 and 340 nm. At 340 nm, the fit gives pK_{ox1} = 7.14 ± 0.26 and pK_{ox2} = 9.32 ± 0.36. The change at 315 nm is best fit for a single deprotonation event, giving pK_{ox1} = 7.82 ± 0.10. The lower wavelength region of the CD spectra was unaffected by pH, indicating that the overall fold of the protein remains unchanged, which is consistent with crystallographic results of trunc*Tt*Rp. The structure of trunc*Tt*Rp crystallized at pH 6.2 is very similar to *Tt*Rp at pH 8.5 and contains only subtle changes localized at the [2Fe-2S] cluster. These titration and structural results further elucidate the histidine ligand characteristics and are consistent with important roles for these amino acids.

Rieske proteins are electron transport proteins that are involved in key biological processes, including respiration and photosynthesis. They function within cytochrome bc_1 (complex III) of the respiratory electron transport chain in both eukaryotes and prokaryotes and in the cytochrome bc_1 complexes of photosynthetic bacteria, as well as in the cytochrome b_6f complex of the plant photosynthetic electron transport chain. There are also Rieske-type proteins that are part of bacterial dioxygenase systems that break down aromatic compounds or serve in detoxification pathways (*1*−*4*).

Rieske proteins have a conserved fold and contain a [2Fe-2S] cluster, with one iron ligated by nitrogens from two solvent-exposed histidine residues and the other iron ligated by sulfurs from two cysteine residues (Figure 1). Rieske proteins couple electron transfer with proton movement across the membrane and thus have pH-dependent reduction potentials. These potentials are positive and can be as high as ∼+400 mV at low pH (*1*). Electrochemical titrations measured as a function of pH result in two pK_a values for the oxidized protein (pK_{ox1} and pK_{ox2}) and one or two pK_a values for the reduced protein (pK_{red}) (see, for example, refs (*5*−*7*)).

The mechanism of the Rieske protein electron transfer is thought to include a large-scale movement of the Rieske domain within the larger complex, between quinol and cytochrome c_1 in complex III of the respiratory chain or between plastoquinol and cytochrome *f* in the photosynthetic electron transfer chain. Rieske proteins oxidize quinol (or plastoquinol) by accepting one of its electrons and a proton and subsequently reduce cytochrome c_1 (or cytochrome *f*). There are several crystal structures of the bc_1 or b_6f complexes in which the Rieske domain either interacts with one of these redox sites or is found in an "intermediate" site (*8*−*16*). One crystal form reveals the Rieske protein interacting directly, via a hydrogen bond, with the propionate group of the cytochrome c_1 heme (*16*). Other structures show interactions between the Rieske protein and inhibitors such as stigmatellin that bind in similar locations to and structurally resemble quinol (see, for example, refs (*8*−*12*, *14*, *15*). Similar interactions can be observed in b_6f complexes (*17*−*19*).

The *Thermus thermophilus* Rieske protein (*Tt*Rp)[1] is thought to be a respiratory-type Rieske protein. Thermodynamic characterization

[†]This work was supported by the Welch Foundation [W-1661 (L.M. H.-W.), W-0031 (Trinity Chemistry Department)], and the Petroleum Research Fund (43999-GB3). Acknowledgment is made to the Donors of the American Chemical Society Petroleum Research Fund for partial support of this research. The CD was acquired and supported by the National Science Foundation (BIO MRI -0718766). S.K.M. and R.P. were supported by summer undergraduate research fellowships provided by Trinity University.

[‡]Protein Data Base ID 3FOU.

*To whom correspondence should be addressed: e-mail, laura.hunsickerwang@trinity.edu; phone, (210) 999-7895; fax, (210) 999-7569.

[1]Abbreviations: LMCT, ligand to metal charge transfer; *Tt*Rp, *Thermus thermophilus* Rieske protein previously characterized; trunc*Tt*Rp, *Tt*Rp less 17 amino acids; EPR, electron paramagnetic resonance; MES, 2-(*N*-morpholino)ethanesulfonic acid hydrate; MOPS, 3-(*N*-morpholino)propanesulfonic acid; HEPES, 4-(2-hydroxyethyl)piperazine-1-ethanesulfonic acid; Tris, 2-amino-2-(hydroxymethyl)-1,3-propanediol; CAPS, 3-(cyclohexylamino)-1-propanesulfonic acid; NaOAc, sodium acetate.

 Published on Web 09/03/2009

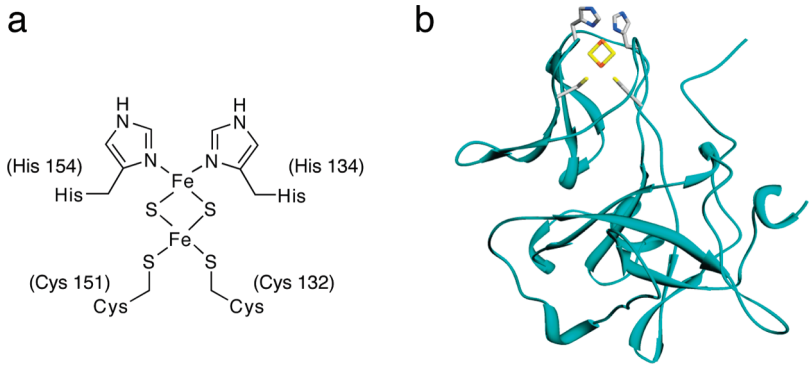

FIGURE 1: (a) Diagram of the [2Fe-2S] cluster with the two histidine ligands (His134 and His154) and the two cysteine ligands (Cys132 and Cys151). (b) Ribbon diagram of the crystal structure of truncated *T. thermophilus* Rieske protein obtained at pH 6.2.

of the protein indicates a low-pH reduction potential of +161 mV with pK_{ox1}, pK_{ox2}, and pK_{red} values of 7.85, 9.65, and 12.5 respectively (*5*, *6*). Crystallographic analysis at higher pH (pH ~8.5, Protein Data Bank entry 1NYK) revealed an overall fold similar to other Rieske proteins, despite its low sequence similarity. In this structure, *Tt*Rp participates in an interesting interprotein hydrogen bond made between histidine residues (His134) in two symmetry-related protein molecules (*20*). Previously published spectroscopic characterization indicates that *Tt*Rp has similar EPR *g* values to other Rieske proteins, with the characteristically low g_{av} = 1.91 (*21*). Furthermore, the visible spectrum of the protein is dominated by three major ligand to metal charge transfer (LMCT) bands at 325, 458, and 560 nm; at least one of these bands shifts with changes in pH (*22*).

[2Fe-2S] clusters in both Rieske and Rieske-type proteins have been studied with circular dichroism. All show features in the visible region that arise from transitions originating from the metal cluster. There are characteristic positive bands near 300−350 and 400−500 nm and a large negative band near 400 nm (*21*, *23*−*26*). Bovine Rieske protein also showed pH-dependent changes in the visible region with increased pH (*23*). Probing this region of the CD spectrum provides a unique spectroscopic window, since the transitions all derive from the iron−sulfur cluster.

To understand how the Rieske proteins function, both structural and functional characterizations are necessary. In the following report, UV−visible and CD spectra at various pH values are used to determine pK_a values of the oxidized protein for both a truncated and the previously characterized version of the *T. thermophilus* Rieske protein in solution using methods other than electrochemical titrations. The truncated version of the protein (trunc*Tt*Rp) was created to achieve a low-pH crystallization condition, and we report here the lower pH structure of trunc*Tt*Rp. This lower pH structure shows subtle structural changes that occur in response to different pH environments. However, there are notable spectroscopic changes that accompany the same different pH environments, consistent with small structural changes localized to the iron−sulfur cluster.

EXPERIMENTAL PROCEDURES

Protein Expression and Purification. The vectors used for the expression of *Tt*Rp and trunc*Tt*Rp were kindly provided by the laboratory of James A. Fee at The Scripps Research Institute. *Tt*Rp is the construct previously described in the literature (*5*, *20*) and is composed of amino acids 38−210, beginning with SLPREEVT and ending with ASAGAYTWRV. The truncated

Scheme 1

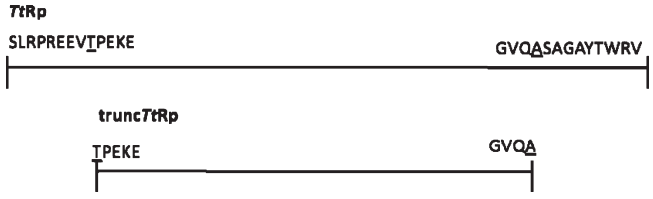

version has the eight N-terminal residues and nine C-terminal residues of *Tt*Rp removed, and thus the protein is composed of amino acids 46−201 (Y. Chen and J. A. Fee, unpublished). The N-terminal amino acid in the truncated protein is T46 and the C-terminus is A201, both underlined in the sequences shown above (Scheme 1).

Both versions of the proteins were expressed and purified as previously reported (*20*). The purity of each protein was assessed by SDS−PAGE gel. The concentration of each *Tt*Rp was determined by the difference in A_{572} of the isolated oxidized form and the reduced form obtained by the addition of an excess of sodium dithionite as described previously (*20*). The absorptivity of the truncated protein was determined to be slightly different than *Tt*Rp, 1441 M^{-1} cm^{-1}. Thus, the concentration of trunc*Tt*Rp was determined in the same way as *Tt*Rp, with the new absorptivity.

pH Titration Assay. All UV−visible data were collected on a Jasco V-530 spectrophotometer (Tokyo, Japan) with a 1 cm path length in quartz microcuvettes. The purified protein was diluted to a final concentration such that the absorbance at 436 nm was in the linear range of the UV spectrophotometer (42.5 μM for *Tt*Rp and 53.4 μM trunc*Tt*Rp) in a final volume of 400 μL of 50 μM appropriate buffer for the desired pH. The buffers used were NaOAc, MES, MOPS, HEPES, Tris, TAPS, CAPS, NaH_2PO_4, and NaOH. The pH of the buffer was determined immediately before the experiments to account for any drift over time. The samples were allowed to incubate for at least 4 h at 4 °C at the desired pH. For each pH, the spectrum of the protein was measured from 800 to 200 nm in triplicate using the appropriate buffer as a reference. The buffer used for protein storage (50 mM Tris, 100 mM NaCl, pH 8.0) was used to obtain a baseline. The measurement of A_{436} was recorded and normalized to the A_{280}. All chemicals used for the pH titration assays were obtained from Sigma Aldrich Chemical Co. (St. Louis, MO).

CD Titrations. CD spectra were collected on a Jasco J-815 spectropolarimeter (Tokyo, Japan). Experimental conditions used were as follows: bandwidth, 2 nm; scan speed, 500 nm/min; resolution, 1 nm; path length, 1 mm; room temperature,

20−22 °C; response time, 1 s. The samples for the CD titration experiments were prepared similarly to the UV−visible experiments. The purified protein was diluted to a final concentration of 138 μM for spectra taken from 650 to 300 nm and 34.5 μM for the spectra taken 300−200 nm in a final volume of 400 μL of 50 μM appropriate buffer for the desired pH. For each pH, the spectrum of the protein was measured in triplicate. For the reduced and oxidized spectral comparison of *Tt*Rp and trunc*Tt*Rp, the protein concentrations were 138 μM in 20 mM Tris, pH 8.0, and 100 mM NaCl. Dithionite was added to an excess of 100-fold. All chemicals used for the pH titration assays were obtained from Sigma Aldrich Chemical Co. (St. Louis, MO).

Curve Fitting. The pH titration data was graphed using Prism 4.0 (GraphPad Software) and fit using nonlinear regression to an equation representing the sum of two Henderson−Hasselbalch equations for the two pK_a values (*27*). This fit assumes two noninteracting sites. This equation

$$A_{436} = (A_{436})_{max} + \frac{(\text{span } 1)10^{pK_{ox1}-pH}}{1+10^{pK_{ox1}-pH}} + \frac{(\text{span } 2)10^{pK_{ox2}-pH}}{1+10^{pK_{ox2}-pH}}$$

$$\text{span } 1 = y_{min} - y_{pK_{ox1}} \quad \text{span } 2 = y_{pK_{ox2}} - y_{max}$$

fits as a sum of two sigmoids, and span 1 and span 2 reflect the relative span of the sigmoid for the individual pK_a values. $(A_{436})_{min} - (A_{436})_{pK_{ox1}}$ is the span in y between the minimum y value and the maximum y value associated with pK_{ox1}. Likewise, $(A_{436})_{pK_{ox2}} - (A_{436})_{max}$ signifies the change in the y value associated with pK_{ox2}. The fit with the single Henderson−Hasselbalch uses the same formulation as seen above but has only a single pH term and span.

EPR. Protein samples were treated with 30% (v/v) glycerol as a cryoprotectant, reduced with dithionite, and loaded into standard EPR tubes. For the trunc*Tt*Rp and *Tt*Rp preparations, the final concentrations were 1064 and 160 μM, respectively. Spectra were taken at the CalEPR Center at the University of California, Davis, on a Bruker ECS 106 continuous wave X-band spectrometer. Data were collected at 10K in an Oxford ESR 900 liquid helium cryostat using an Oxford ITC503 temperature controller. Field calibration was done at room temperature using g-value marker LiF:Li (g = 2.002293).

X-ray Crystallography. A well solution made of PEG 8000 (8−14%), sodium cacodylate, pH 6.21 (100−275 mM), and calcium acetate (225−275 mM) was added to a 40 mg/mL trunc*Tt*Rp in a 1:1 ratio, usually with 1 μL each. From 1.25 to 1.75 μL of 0.1 M praseodymium(III) acetate (Hampton Research) was added to the sitting drop in a polystyrene bridge. Crystals were grown at room temperature and consistently formed within 24 h. The crystal was pulled into a loop from its mother liquor and then swiped through a mixture of 1:1 paraffin oil/Paratone-N ((*28*); Hampton Research) before flash cooling. Poorly formed crystals will appear without the praseodymium salt, but the crystal quality and reproducibility greatly increased with addition of the heavy atom. The salt was identified through an additive screen (Hampton Research).

Data were collected on a Rigaku MicroMax 007HF X-ray generator equipped with R-AXIS HTC imaging plates in the X-ray Crystallography Core Laboratory at the University of Texas Health Science Center at San Antonio. The data were integrated and scaled using HKL-2000 (*29*), and data collection statistics are listed in Table 1. The structure was solved by molecular replacement using protein A of the higher pH crystal structure of *T. thermophilus* Rieske protein (1NYK) using Molrep (*30*). The structure was refined with Refmac 5 (*31*), and the electron density maps were fit using Xfit (*32*). Refinement statistics are summarized in Table 2. The final structure and structure factors have been deposited in the PDB with code 3FOU (Table 2).

Table 1: Data Collection Statistics

unit cell parameters	
a, b, c (Å)	113.152, 58.512, 58.798
$\alpha = \beta = \gamma$ (deg)	90
space group	$P2_12_12$
wavelength (Å)	1.54
resolution (Å)	58.8−2.10 (2.15−2.10)[a]
total observations	105184
unique observations	23456
redundancy	4.5
completeness (%)	99.7 (98.7)
$I/\sigma I$	13.1 (2.5)
R_{sym}	0.088 (0.529)

[a]Values in parentheses correspond to the highest resolution bin.

Table 2: Refined Model Statistics and *B* Values

refined model statistics	
residue range	46−201
no. of non-H atoms (in asymmetric unit)	2473
no. of water molecules	114
no. of Fe atoms	4
no. of Pr atoms	6
no. of Ca atoms	2
R (%)	19.8
R_{free} (%)	24.6
rmsd from ideal, bond lengths (Å)	0.02
rmsd from ideal, angles (deg)	1.86
esu, bond lengths (Å)	0.18
average B values (Å^2)	
overall	37.8
protein atoms (molecule A, molecule B)	38.0, 37.0
main chain (molecule A, molecule B)	37.2, 36.0
side chain (molecule A, molecule B)	39.1, 38.1
metal cluster (molecule A, molecule B)	30.4, 30.9
Pr ions	54.5
water molecules	39.1
Ramachandran plot	
residues in most favored regions (%)	88.7
residues in additionally allowed regions (%)	11.3
PDB ID	3FOU

RESULTS

Spectroscopic Characterization of TtRp and truncTtRp. *Tt*Rp is the soluble version of the Rieske protein from *T. thermophilus* that has been previously reported and characterized in the literature (*5*, *6*, *20*−*22*). trunc*Tt*Rp is a shortened version of *Tt*Rp that lacks the N-terminal eight residues and C-terminal nine residues, which was constructed to aid in crystallization (see Scheme 1 and Crystal Structure below). UV−visible data for the "as isolated" protein for both *Tt*Rp and trunc*Tt*Rp in the oxidized and reduced forms are nearly identical and compare with the previously reported values (Table 3) (*21*). EPR spectra of *Tt*Rp and trunc*Tt*Rp show that the two proteins have identical g values, which also match previously reported values (Figure 2a) (*21*). CD spectra of the oxidized and reduced *Tt*Rp and trunc*Tt*Rp are shown in Figure 2b. They are nearly indistinguishable and match previously reports of *Tt*Rp (*21*). Thus, the proteins do not differ significantly in electronic structure.

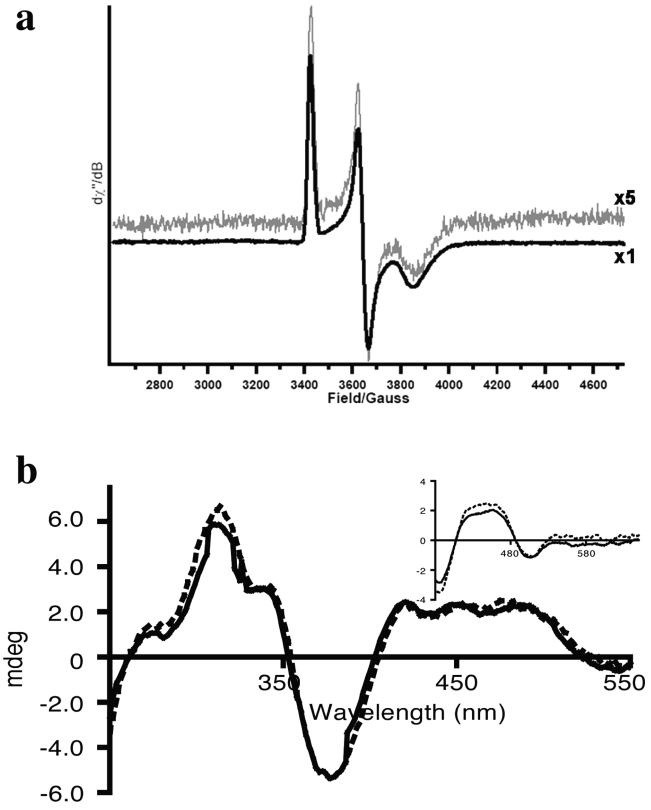

FIGURE 2: (a) EPR spectra of the trunc*Tt*Rp (black) and *Tt*Rp (gray). EPR parameters: temperature, 10 K; microwave frequency, 9.696 GHz (*Tt*Rp) and 9.693 GHz (trunc*Tt*Rp); microwave power, 50 μW; modulation frequency, 100 kHz; modulation amplitude, 8 G; sweep time, 41.94 s; 1024 points per spectrum; four scans each. The *Tt*Rp trace is multiplied by a factor of 5 to match protein concentration. (b) Circular dichroism spectra for oxidized *Tt*Rp (solid line) and trunc*Tt*Rp (dotted line) from 650 to 200 nm. The inset is reduced *Tt*Rp (solid line) and trunc*Tt*Rp (dotted line) from 650 to 380 nm. The proteins were reduced by addition of a 100-fold excess of dithionite.

Table 3: *Tt*Rp and trunc*Tt*Rp Visible λ_{max} Values

protein	oxidation state	λ_{max} (nm)
trunc*Tt*Rp	oxidized	328
		458
		564 (s)
	reduced	426
		516
*Tt*Rp[a]	oxidized	325
		458
		560 (s)
	reduced	425
		550

[a]Values taken from ref *21*, which also match those obtained in our laboratory with this protein.

A spectroscopic analysis of the changes that occur in this protein as a function of pH can be achieved by monitoring the UV−visible spectrum at different pH values. There are three major LMCT bands seen in the oxidized protein at 325, 458, and a shoulder at 560 nm. Upon raising the pH, the 458 nm band shifts to 436 nm and increases in intensity. The 325 nm band also increases in intensity. These changes are consistent with a previous report (*22*). The data reported here represent a full characterization of these changes for both *Tt*Rp and trunc*Tt*Rp, resulting in measurable pK_{ox1} and pK_{ox2} values. Representative spectra from the pH titrations with the observed changes in λ_{max} and plots of the changes in A_{436} versus pH for both proteins are shown in Figure 3. The A_{436} versus pH plots are fit with a sum of two Henderson−Hasselbalch equations and result in two oxidized pK_a values. For *Tt*Rp pK_{ox1} = 7.48 ± 0.12 and pK_{ox2} = 10.07 ± 0.17 and for trunc*Tt*Rp pK_{ox1} = 7.87 ± 0.17 and pK_{ox2} = 9.84 ± 0.42 (Table 4). The values for the absorbances at 436 nm for trunc*Tt*Rp do not differ significantly upon an increase in ionic strength to 2 M NaCl (data not shown), indicating that these spectroscopic changes are not due to electrostatic interactions.

The sum of the Henderson−Hasselbalch equations was chosen to fit the UV−visible titration since it is the simplest interpretation of the data. This fit assumes two noninteracting sites and is based on previous work using NMR chemical shifts (*27*). Neither adding a Hill coefficient to the fits nor adding a mathematical cross-term of the two Henderson−Hasselbalch terms improves the fitting statistics significantly. Thus, the simple sum equation best fits all of the UV−visible data.

For *Tt*Rp, the pK_{ox1} and pK_{ox2} values are more separated than those reported in the literature obtained through electrochemical measurements, with pK_{ox1} slightly lower and pK_{ox2} slightly higher. The difference between the pK_a values for *Tt*Rp using the UV−visible titration data (pK_{ox2} − pK_{ox1} = ΔpK_{ox}) is 2.6, whereas the difference from the literature values is ΔpK_{ox} = 1.8 (*5*). The trunc*Tt*Rp values are actually closer to the literature values for *Tt*Rp in both the actual pK_a values and the ΔpK_{ox} = 2.0. In the data for *Tt*Rp, there is a larger spread between pK_{ox1} and pK_{ox2}, which may indicate more of a cooperative effect, but accounting for this in the fit using a Hill coefficient does not significantly improve the fit or the match to the literature values. Overall, these pK_a values are similar to the literature, and the small differences may reflect slight changes in the protein stability or dynamics and/or may be due to the different experimental conditions in the electrochemical studies (*5*) and the UV−visible titrations reported here.

The circular dichroism spectra for trunc*Tt*Rp have been taken at both low wavelength (220−300 nm) and at high wavelength (300−650 nm) in order to capture the structural information for both the global protein fold and the electronics of the cluster (Figure 4) (*34*). In the low wavelength region, there is no change in the spectrum upon increasing pH (Figure 4a), indicating that there is no large, global conformational change in the protein as the pH changes. However, there are changes in peak intensity and wavelength observed for the visible region. The spectra at the visible wavelengths are reporting on differences in absorbance of the right and left polarized light by the [2Fe-2S] cluster, and thus these pH-dependent changes in ellipticity reflect changes in the cluster environment. Notably, the changes in ellipticity at 315 and 340 nm can be fit as a function of pH (Figure 4c,d). The change at 340 nm was fit in the same manner as the UV−visible data, using a sum of two Henderson−Hasselbalch equations. Such treatment results in two pK_a values, pK_{ox1} = 7.14 ± 0.26 and pK_{ox2} = 9.32 ± 0.36. However, the change at 315 nm is best fit to a single Henderson−Hasselbalch equation, giving pK_{ox1} = 7.82 ± 0.10 (Table 4). These values again match well with the previously reported pK_a values determined by electrochemical titrations (*5*). Interestingly, the change at 315 nm is best fit with a single pK_a that is very close to pK_{ox1} from both the 340 nm data and the UV−visible titration experiments. Addition of the second pK_a term did not improve the fit and resulted in nonsense values for pK_{ox2}. One interpretation of this result is that the 315 nm band is reporting solely on the first deprotonation event.

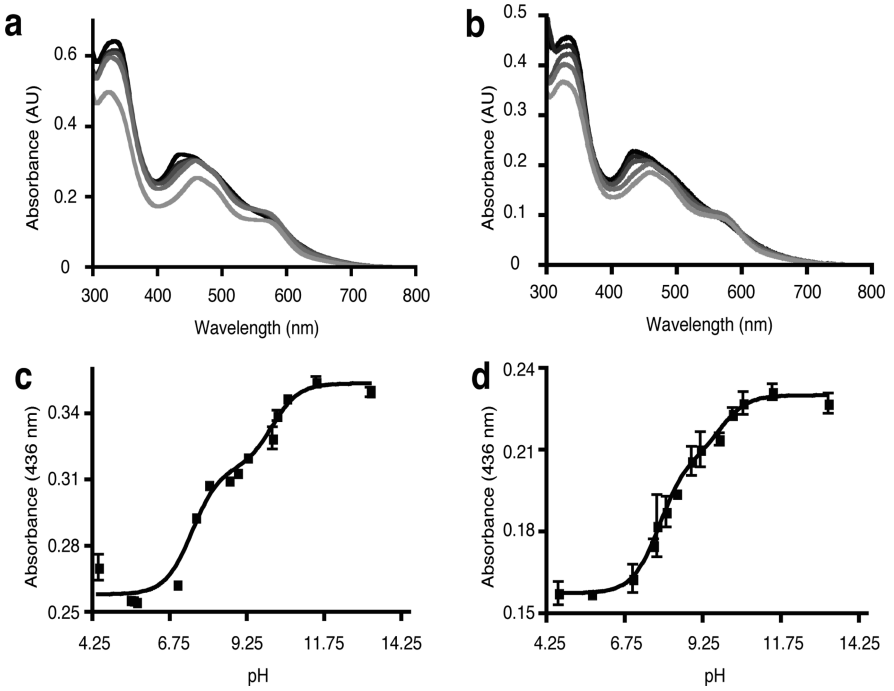

FIGURE 3: (a, b) UV−vis spectra of the pH titration of *TtRp* (a) and trunc*TtRp* (b). The spectra are shown from 800 to 300 nm. The absorbance peak at 436 nm increases as the pH value is increased. (c) and (d) are plots of the A_{436} vs pH for *TtRp* (c) and trunc*TtRp* (d). Errors shown are standard error of the mean from experiments done in triplicate. The curve fit is the simple sum of two Henderson−Hasselbalch equations (see Experimental Procedures).

Table 4: Measured Oxidized pK_a Values for *Tt*Rp and trunc*Tt*Rp

method	protein λ (nm)	pK_{ox1}	pK_{ox2}	span 1 (Abs units)	span 2 (Abs units)	Y_{max} (Abs units)
UV−vis	*Tt*Rp 436	7.48 ± 0.12	10.07 ± 0.17	−0.057 ± 0.003	−0.039 ± 0.004	0.35 ± 0.003
	trunc*Tt*Rp 436	7.87 ± 0.17	9.84 ± 0.42	−0.050 ± 0.003	−0.023 ± 0.006	0.23 ± 0.003
CD	trunc*Tt*Rp 340	7.14 ± 0.26	9.32 ± 0.36	−0.795 ± 0.125	−0.530 ± 0.126	3.75 ± 0.06
	trunc*Tt*Rp 315	7.82 ± 0.10		1.42 ± 0.06		4.92 ± 0.04

Crystal Structure of the Truncated T. thermophilus Protein at Low pH. trunc*Tt*Rp was crystallized at an acidic pH of 6.2, data were collected to 2.1 Å resolution, and the model was refined to a final R = 19.8 and R_{free} = 24.6 (Figure 5, Table 2). To achieve this crystal form, the protein was shortened, removing the eight N-terminal and nine C-terminal residues (see Experimental Procedures, Scheme 1). The previously reported structure of *Tt*Rp at higher pH (8.5) included these 17 residues in the sequence, but they were disordered and not visible in the electron density (*20*). Thus, the residues were removed from the construct, and the new crystallization conditions were determined. *Tt*Rp does not readily crystallize under the lower pH condition, and trunc*Tt*Rp will only form plates under the higher pH conditions reported previously (*20*).[2]

The lower pH crystal form has several notable characteristics. First is the presence of 6 Pr^{3+} ions found in the structure resulting from addition of the lanthanoid to the crystallization condition (Figure 5a). These large cations make cross-protein interactions between proteins and symmetry-related proteins representing important crystal contacts. The oxophilic Pr^{3+} ions are ligated by surface Glu and Asp residues, with their coordination shells filled out by H_2O and, in two cases, acetate molecules. These sites have the typical six to nine ligands per metal seen for lanthanoids. The ions can be readily detected in an anomalous difference Patterson map. Interestingly, one Pr^{3+} appears to be disordered and has a 0.5 occupancy in two different sites, which are adjacent to another fully occupied Pr^{3+}.

There are two proteins in the asymmetric unit, and they will be referred to as proteins A and B. A notable difference between them is a hydrogen bond that is formed between the Nε of His154, one of the ligands to the [2Fe-2S] cluster of protein A in the asymmetric unit, and the carboxylate group of the C-terminal alanine in a symmetry-related protein (Ala201 A′). One oxygen of the carboxylate group is within 2.6 Å of the His154 A Nε, indicating a hydrogen bond (Figure 5b). There is, therefore, one hydrogen shared between the N and O. There is also an adjacent lysine amino group (Lys68 B Nζ) in protein B of the asymmetric unit that interacts with the C-terminus, balancing the charge effect of the carboxylate. The hydrogen bond between the carboxylate and His154 A is likely an important crystal contact and, if so, could indicate why *Tt*Rp does not crystallize under these specific conditions. The longer *Tt*Rp C-terminus would presumably be in a different position and thus not be available to make this contact. Protein A differs slightly from protein B, and an overlay of the two proteins results in an rmsd of 0.26 Å (Supporting Information, Table S1). The above-mentioned interaction between the terminal carboxylate group and His154 A Nε

[2]Interestingly, trunc*Tt*Rp also crystallized under an alternate condition at pH 4.6 in PEG 400 and acetate, but data collected on this form consistently showed degradation of the iron−sulfur cluster (L. Hunsicker-Wang, J. A. Fee, and C. D. Stout, unpublished).

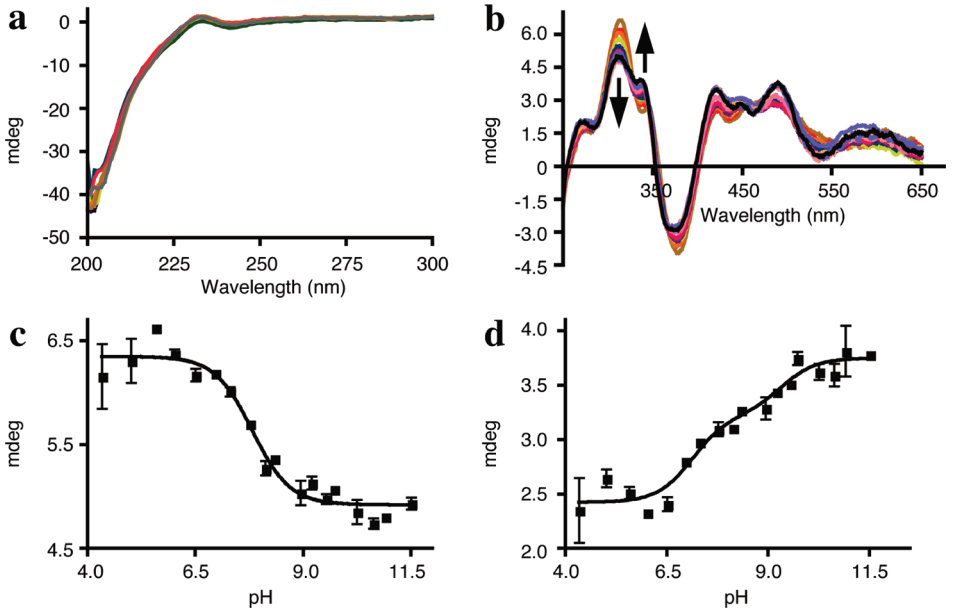

FIGURE 4: pH-dependent CD spectra. (a) Low wavelength region (300−200 nm) of trunc*Tt*Rp at 34.5 μM with increasing pH. (b) Visible wavelength region (650−300 nm) of trunc*Tt*Rp at 138 μM with increasing pH. Arrows indicate direction of change with increasing pH at 315 and 340 nm, and the black spectrum is for the highest pH. (c) and (d) are plots of millidegrees of rotation with increasing pH at 315 and 340 nm, respectively. Errors shown are standard error of the mean from experiments done in triplicate. The curve fit is the simple sum of two Henderson−Hasselbalch equations for 340 nm and single Henderson−Hasselbalch equation for 315 nm (see Experimental Procedures).

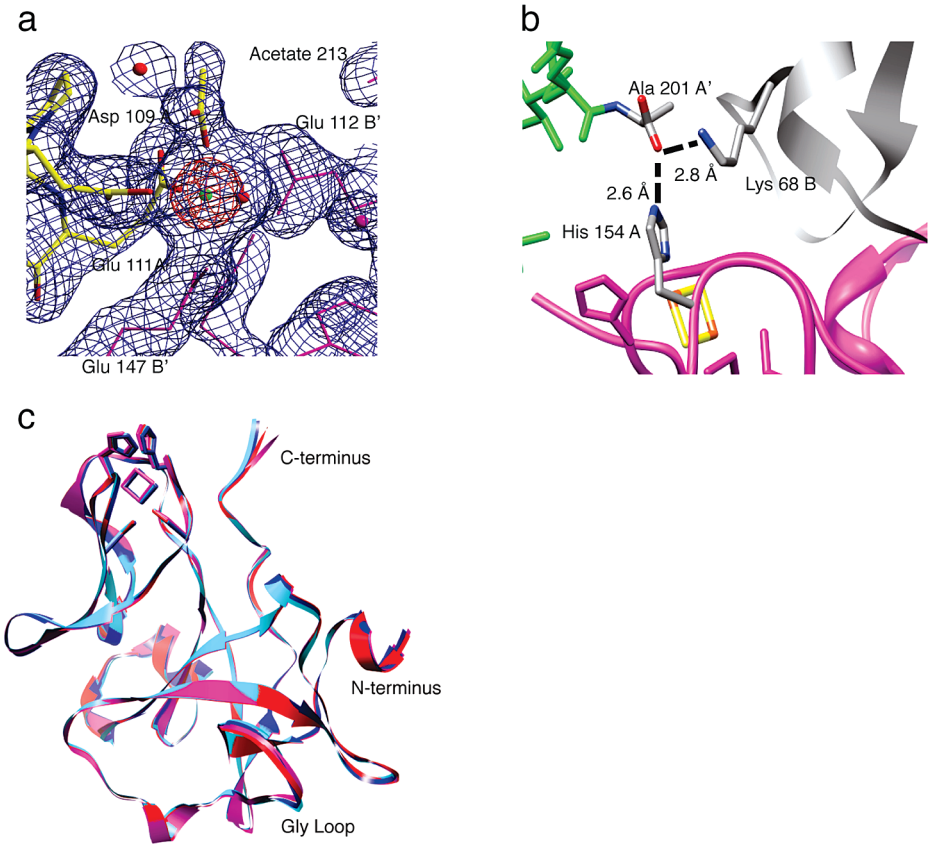

FIGURE 5: (a) Electron density map of truncated *T. thermophilus* Rieske protein at Pr 206. Blue density is 1σ and red is 5σ. Atoms from copy A of the protein in the asymmetric unit are colored by atom, and the symmetry-related protein atoms are in magenta and labeled as B′. Waters are depicted as red spheres. (b) Interaction between His154 and the C-terminus of the symmetry-related protein. One of the oxygen atoms of the carboxy terminus of a symmetry-related protein (A′, green wire) makes a hydrogen bond with Nε of His154 of protein A (magenta ribbon). Protein B (gray ribbon) in the asymmetric provides an adjacent Lys68. Interacting residues are represented as sticks and colored by atom. (c) Overlay of the *T. thermophilus* Rieske protein crystallized at high pH (A and B of 1NYK) and of the truncated *T. thermophilus* Rieske protein crystallized at low pH (A and B of 3FOU) using global best fit in Chimera. The lower pH A and B proteins are shown in red and pink, respectively, and the higher pH A and B proteins are shown in blue and cyan, respectively. The [2Fe-2S] and the four ligands are shown as sticks.

is only present in protein A. In protein B, the only other cluster interaction is a hydrogen bond of His134 B Nε with an ordered water molecule.

Comparison between the Low pH and High pH T. thermophilus Structure. The Rieske protein structure previously reported was produced with the longer protein (*Tt*Rp) in crystallization conditions at pH 8.5. This crystal structure also had two proteins in the asymmetric unit. A comparison between all four copies of the proteins, two at lower pH and two at higher pH, is shown in Figure 5c. All alignments were made using Chimera (*35*). Aligning the proteins with a global overlay indicates only minor changes between the higher and lower pH structures, but there are differences in backbone structure at the C-terminus and in a glycine-rich loop (Gly63−65) (Figure 5c). Upon further inspection, however, there are subtle changes at the [2Fe-2S] cluster including changes in the His Nδ−Fe2−Nδ His angle and some dihedral angles that govern the relative positioning of the histidine residues with respect to each other (Supporting Information, Table S2). The His134 Nδ−Fe2−Nδ His154 angle in Rieske proteins is generally found to be near 90° (see, for example, refs *20*, *36*, and *37*). In protein B of the lower pH structure, this angle is more acute than in the other three proteins (89.7° versus 94°).[3] There is also a 10° difference in a dihedral angle in His 134 between the lower and higher pH structures (Supporting Information, Table S2).

These changes in the geometric measurements of the cluster are small but seem to be the most notable differences between the lower and higher pH structures. The low-pH structure reported here is of lower resolution (2.1 Å) and was refined with a different program than the high pH structure, so care must be taken in interpreting the small differences in the metrics of the cluster. These changes in metrics could be within the limits of the error of the measurements at this resolution and using these programs. However, the minor changes observed are consistent with the solution CD results in the low wavelength region that indicate that only minor changes *should* be observed in the crystalline state since no large changes in protein conformation were detected.

DISCUSSION

Iron−sulfur proteins conveniently contain an analytical handle for UV−visible and CD spectroscopies, the metal cluster itself. Rieske proteins have an observable signal in the visible region (500−300 nm) that is assigned as LMCT bands. We utilized these bands to examine the molecular environment of the [2Fe-2S] cluster of the oxidized Rieske proteins over a range of pH (*4*−*12*) with standard UV−visible and CD spectroscopies. In doing so, we were able to determine the two pK_a values for the oxidized protein in a facile and nondestructive manner. The pK_a values obtained through the titrations are unique because they are determined *solely* in the oxidized state. Previous measurements of these pK_a values have all been obtained through more arduous electrochemical means, which experimentally probe changes between the reduced and oxidized states. Small differences between the reported pK_a values from the previous electrochemical measurements and the spectrophotometric measurements reported here could be due to experimental differences (*5*).

The UV−visible pH titration spectra of both trunc*Tt*Rp and *Tt*Rp result in a change to the 458 nm LMCT band, in that it shifts to a shorter wavelength, λ_{max} 436 nm, and increases in intensity. This shift to lower wavelength would be consistent with deprotonation of the histidine ligands. Conversion of a protonated histidine (neutral) ligand to a deprotonated "imidazolate" (anionic) ligand would cause a strengthening and shortening of the Fe−Nδ bond(s), since the "imidazolate" ligand would be a better σ donor than the neutral form of histidine (*38*). In a qualitative assessment, electrons in the *lower relative* energies of ligand-based orbitals (due to the strengthening of the Fe−N bonds) are excited into the metal-based orbitals, resulting in a shift to higher energy for the observed LMCT band(s) (*39*). The modest increase in molar absorptivity is also consistent with greater electron density at the histidine ligands which would increase the probability that the LMCT occurs.

The CD data are also consistent with a model of histidine deprotonation. The changes in the CD spectra are confined to the visible wavelengths, which solely report on the electronics of the cluster (*40*). The lower wavelength region, which reports on protein global structure, does not change. Therefore, the changes due to increasing pH must be localized to the cluster region. The histidines are the closest, solvent-exposed, titratable groups to the cluster and are thus the most likely groups to be sensitive to pH.

The *T. thermophilus* Rieske protein crystal structures at two different pH values represent structures below and above pK_{ox1} of the protein. In solution, the protein has different UV−visible and CD spectra (see Supporting Information, Figure S1) at pH 6.5 than at pH 8.6, consistent with different protonation states of the histidines. However, the micro pH environment of the crystallization drop cannot be measured, and the H atoms cannot be located at this resolution. Thus one cannot know the exact protonation state of the hisitidine. The most likely states, though, are that the lower pH structure would be fully protonated, while the higher pH structure would be a singly deprotonated state. Comparing them allows a glimpse into protein conformation changes that *may* occur as a function of protonation state. Since reduction of the protein requires protonation (at moderate pH), it is possible that the lower pH structure may mimic the reduced state. Thus, the small, localized changes at the cluster may be similar to those motions occurring as the protein is reduced and protonated through its catalytic mechanism *in vivo*.

In the bovine bc_1 complex crystal structures, the Rieske protein either interacts with the redox centers (quinol or cytochrome c_1) or is in intermediate states (*16*). When the Rieske protein interacts with the cytochrome c_1 in the bovine bc_1 complex, His161 (equivalent to His154 in *Tt*Rp) hydrogen bonds to the propionate group of the heme moiety (Figure 6a). In an intermediate state conformation, "Int", the structure opens, allowing solvent to interact with residues that make up the interface between the large domain and the cluster-binding domain. In addition, a proline in the "Pro loop" isomerizes from the normal *trans* conformation to a *cis* conformation (*16*).

The crystal structure of the solubilized bovine Rieske protein (1RIE) is identical to the form interacting with cytochrome c_1 (*36*). The higher pH structures of *Tt*Rp (*20*) (1NYK) have the smallest rmsd with this protein (1.16 Å), closely followed by protein A in the lower pH structure (rmsd 1.17 Å) (Supporting Information, Table S1). None of the *T. thermophilus* structures show a *cis*-proline isomerization, nor do they show the larger changes in structure observed in the "Int", open state within the bovine bc_1 complex. Therefore, the higher pH structure is most representative of the closed "c_1" conformation, followed closely by protein A in the lower pH structure.

[3] *B* values for this residue are 31 Å^2 and are slightly better than those for the entire protein, 36.9 Å^2. Thus, it is not poor placement or disorder of the residue that results in the unusual angle.

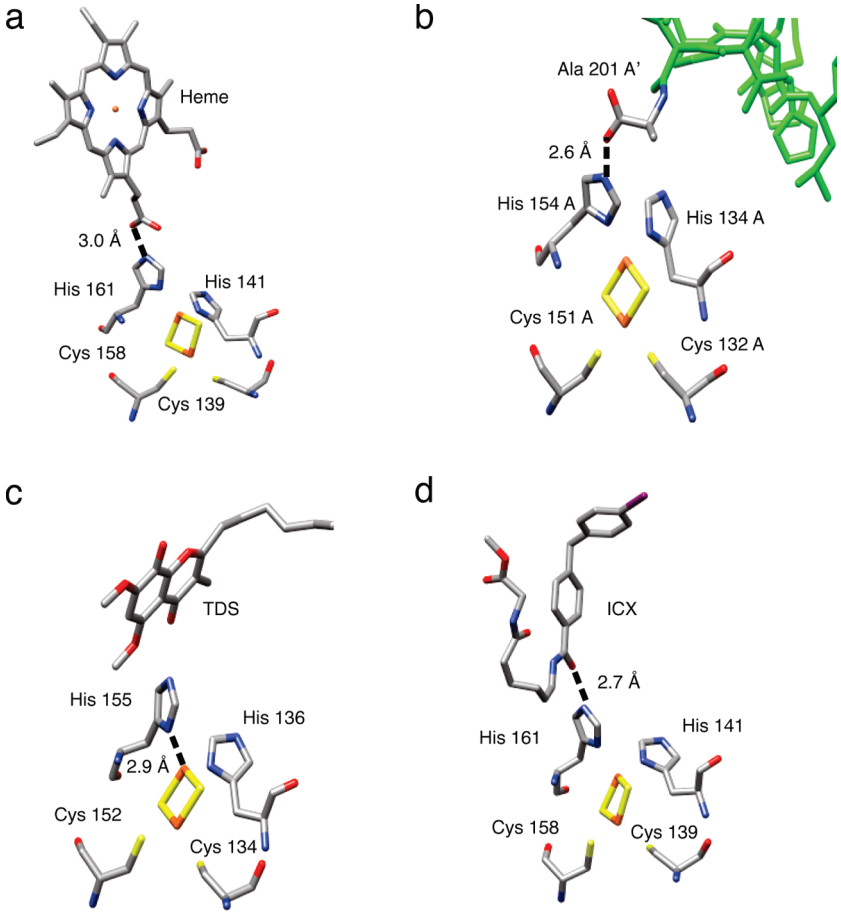

FIGURE 6: Various interactions of [2Fe-2S] ligand histidines with other molecules. (a) Stick diagram showing the interaction of His161 of the Rieske domain interacting with the heme propionate of the bovine cytochrome bc_1 complex (1BE3). (b) Stick diagram showing the interaction of His154 of trunc*Tt*Rp crystallized at low pH with the C-terminal alanine (colored by atom) of a symmetry-related protein (green). (c) Stick diagram of His155 interacting with a carbonyl of the inhibitor tridecylstigmatellin (color by atom) in the cytochrome b_6f complex of *Chlamydomonas reinhardtii* (PDB code 1Q90). (d) Stick diagram of His161 interacting with a carbonyl of the polyketide inhibitor methyl *N*-[(5*Z*)-6-({[4-(4-iodobenzyl)phenyl]carbonyl}amino)hex-5-enoyl]glycinate (color by atom) in the cytochrome bc_1 complex of chicken (3CWB).

Protein A of the lower pH structure is the copy of the protein that has a hydrogen bond between His154 A Nδ and the C-terminal carboxylate group of the symmetry-related protein. Though this hydrogen bond in our structure is a protein crystal packing effect, it does mimic the histidine−propionate group interaction seen in the bc_1 structure (Figure 6a,b) (*16*). Thus, some crystallographically observed interactions of the histidines may give clues as to the roles of these amino acids in the mechanism of the Rieske protein.

A survey of the crystal structures of soluble Rieske structures and bc_1 and b_6f complexes shows a variety of types of observed interactions of the histidine ligands. Within the bc_1 and b_6f complexes the histidines have been shown to interact with quinol mimics, such as stigmatellin (*8*, *11*, *12*, *14*, *15*, *41*) or its derivatives (*17*) at the exocyclic oxygen (Figure 6c). The Rieske−stigmatellin interaction is extremely interesting in light of recent evidence suggesting that binding of stigmatellin results in reduction of the [2Fe-2S] cluster, by an unidentified electron source postulated to be an aromatic side chain (*42*). Having a reduced protein in this position is still consistent as the reduced protein is necessarily protonated and capable of hydrogen bonding to the stigmatellin exocyclic oxygen. Other examples of histidine interactions include hydrogen bonding to the carbonyl oxygen of the protein backbone (Figure 6d) to an inhibitor or to water (*10*, *13*, *18*, *20*, *36*, *43*, *44*). Another crystallographically observed interaction is the His134 Nε−Nε His134′ hydrogen bond in the high-pH *T. thermophilus* structure (*20*).

Taken together, these examples depict the varied types of protein interactions possible with a solvent-exposed histidine ligand in a [2Fe-2S] cluster protein. Through evolution, histidine ligands may have been retained in Rieske proteins since they lend more possible types of protein−protein interactions at the cluster site than if the histidines were, for example, cysteine ligands, as are found in other [2Fe-2S] ferredoxins. Histidine ligands also provide a possible titratable group directly interacting with the [2Fe-2S] cluster and have been shown to greatly alter reduction potential upon mutation to Cys (*45*). The diversity of observed interactions, along with the pH dependence of the UV−visible and CD spectra of the *T. thermophilus* Rieske protein, is consistent with the model in which the histidines are the ionizable groups that are probed when the Rieske proteins are subjected to different pH values.

Spectroscopic evidence further describes the role of histidines in the pH-dependent behavior of the protein (*46*−*48*). pH-dependent shifts of the ^{15}N NMR chemical shifts of ^{15}N-labeled histidines yielded pK_a values of 7.46 and 9.24 that agree with the previously reported pK_a values (*46*) giving very strong evidence for histidine deprotonation. A resonance Raman band at 274 cm^{-1} increases in intensity as the pH is raised (*47*). There are also reported imidazolate signatures in the ATR-FTIR spectra of the Rieske protein from bovine (*48*). Indeed,

DFT/MEAD calculations that model the redox-dependent behavior using the histidines ligated to the cluster closely reproduce the observed pK_a values (*49*). Arguments against the titratable group being the histidine ligands include the fact that the second pK_a of a free histidine is estimated at ~14 based on measurement of free imidazole (*50*), which would make this pK_a inaccessible at physiological pH. However, ligating a to the Lewis acid, Fe^{3+}, can lower the pK_a (*51*). It is possible that the [2Fe-2S] cluster may lower the pK_a values of the ligating histidines enough to exhibit the observed values for the Rieske protein. This line of reasoning has been used to explain other metallosystems (*52*). Obviously, more direct methods to determine if the histidine ligands do indeed lose protons during titration are necessary and underway.

In summation, the UV−visible spectra of this protein change as the pH is increased, and at least one λ_{max} shifts to a shorter wavelength and increases in intensity. This shift to shorter wavelength coupled with an increase in intensity is consistent with a model in which the cluster histidines become deprotonated as pH increases. pH-dependent CD data taken in the visible wavelength ranges are also observed, but no change is observed in the lower wavelength range, which reports on secondary structure element content. Thus, there are no global changes in conformation with increased pH, but there are changes in the cluster electronics. Only small conformational changes localized at the cluster are observed in the crystal structures of the Rieske protein from *T. thermophilus* at two different pH values. A survey of the current Rieske structures points to a broad range of histidine−ligand interactions with other proteins or with small molecules. The CD and UV−vis titration results, the observed changes in the cluster measurements and orientations, and an analysis of the observed interactions in soluble Rieske structures and bc_1 and b_6f complexes signify a wide variety of characterized histidine−ligand interactions, suggesting important roles for these amino acids in both the structure and the function of Rieske proteins.

ACKNOWLEDGMENT

We thank the laboratory of James A. Fee at the Scripps Research Institute for providing the vectors for both *Tt*Rp and trunc*Tt*Rp. We acknowledge specifically Ying Chen, who did the cloning work to make trunc*Tt*Rp. Emily Whitney of Trinity University is acknowledged for determining the new molar absorptivity of trunc*Tt*Rp. We thank Dr. P. John Hart for use of the X-ray facilities at the University of Texas Health Science Center in San Antonio. We also thank Dr. Bert Chandler for helpful discussions.

SUPPORTING INFORMATION AVAILABLE

A figure depicting the differences in the UV−visible and CD spectra at pH values similar to the crystallization conditions, a table with detailed metrics of the cluster, and a table with the rmsd values for the higher and lower pH proteins as well as a comparison to the bovine Rieske protein (1RIE). This material is available free of charge via the Internet at http://pubs.acs.org.

REFERENCES

1. Link, T. A. (1999) The Structures of Rieske and Rieske-Type Proteins. *Adv. Inorg. Chem. 47*, 83–157.
2. Trumpower, B. L., and Gennis, R. B. (1994) Energy Transduction by Cytochrome Complexes in Mitochondrial and Bacterial Respiration: The Enzymology of Coupling Electron Transfer Reactions to Transmembrane Proton Translocation. *Annu. Rev. Biochem. 63*, 675–716.
3. Crofts, A. R. (2004) The Cytochrome bc_1 Complex: Function in the Context of Structure. *Annu. Rev. Physiol. 66*, 689–733.
4. Berry, E. A., Guergova-Kuras, M., Huang, L. S., and Crofts, A. R. (2000) Structure and Function of Cytochrome *bc* Complexes. *Annu. Rev. Biochem. 69*, 1005–1075.
5. Zu, Y., Fee, J. A., and Hirst, J. (2001) Complete Thermodynamic Characterization of Reduction and Protonation of the bc_1-Type Rieske [2Fe-2S] Center of *Thermus thermophilus*. *J. Am. Chem. Soc. 123*, 9906–9907.
6. Zu, Y., Couture, M. M., Kolling, D. R. J., Crofts, A. R., Eltis, L. D., Fee, J. A., and Hirst, J. (2003) Reduction Potentials of Rieske Clusters: Importance of the Coupling between Oxidation State and Histidine Protonation State. *Biochemistry 42*, 12400–12408.
7. Leggate, E. J., and Hirst, J. (2005) Roles of the Disulfide Bond and Adjacent Residues in Determining the Reduction Potentials and Stabilities of Respiratory-Type Rieske Clusters. *Biochemistry 44*, 7048–7058.
8. Solmaz, S. R., and Hunte, C. (2008) Structure of Complex III with Bound Cytochrome *c* in Reduced State and Definition of a Minimal Core Interface for Electron Transfer. *J. Biol. Chem. 283*, 17542–17549.
9. Hunte, C., and Michel, H. (2002) Crystallization of Membrane Proteins Mediated by Antibody Fragments. *Curr. Opin. Struct. Biol. 12*, 503–508.
10. Lange, C., Nett, J. H., Trumpower, B. L., and Hunte, C. (2001) Specific Roles of Protein-Phospholipid Interactions in the Yeast Cytochrome bc_1 Complex Structure. *EMBO J. 20*, 6591–600.
11. Esser, L., Gong, X., Yang, S., Yu, L., Yu, C. A., and Xia, D. (2006) Surface-Modulated Motion Switch: Capture and Release of Iron-Sulfur Protein in the Cytochrome bc_1 Complex. *Proc. Natl. Acad. Sci. U.S.A. 103*, 13045–10350.
12. Huang, L. S., Cobessi, D., Tung, E. Y., and Berry, E. A. (2005) Binding of the Respiratory Chain Inhibitor Antimycin to the Mitochondrial bc_1 Complex: A New Crystal Structure Reveals an Altered Intramolecular Hydrogen-Bonding Pattern. *J. Mol. Biol. 351*, 573–597.
13. Hunte, C., Koepke, J., Lange, C., Rossmanith, T., and Michel, H. (2000) Structure at 2.3 Å Resolution of the Cytochrome *bc*(1) Complex from the Yeast *Saccharomyces cerevisiae* Co-Crystallized with an Antibody F_v Fragment. *Structure 8*, 669–684.
14. Berry, E. A., Huang, L. S., Saechao, L. K., Pon, N. G., Valkova-Valchanova, M., and Daldal, F. (2004) X-Ray Structure of *Rhodobacter capsulatus* Cytochrome *bc*(1): Comparison with its Mitochondrial and Chloroplast Counterparts. *Photosynth. Res. 81*, 251–275.
15. Zhang, Z., Huang, L., Shulmeister, V. M., Chi, Y. I., Kim, K. K., Hung, L. W., Crofts, A. R., Berry, E. A., and Kim, S. H. (1998) Electron Transfer by Domain Movement in Cytochrome bc_1. *Nature 392*, 677–684.
16. Iwata, S., Lee, J. W., Okada, K., Lee, J. K., Iwata, M., Rasmussen, B., Link, T. A., Ramaswamy, S., and Jap, B. K. (1998) Complete Structure of the 11-Subunit Bovine Mitochondrial Cytochrome bc_1 Complex. *Science 281*, 64–71.
17. Stroebel, D., Choquet, Y., Popot, J. L., and Picot, D. (2003) An Atypical Hæm in the Cytochrome *b*(*6*)*f* Complex. *Nature 426*, 413–418.
18. Yamashita, E., Zhang, H., and Cramer, W. A. (2007) Structure of the Cytochrome b_6f Complex: Quinone Analogue Inhibitors as Ligands of Heme C_n. *J. Mol. Biol. 370*, 39–52.
19. Baniulis, D., Yamashita, E., Zhang, H., Hasan, S. S., and Cramer, W. A. (2008) Structure-Function of the Cytochrome *bf* Complex. *Photochem. Photobiol. 84*, 1349–1358.
20. Hunsicker-Wang, L. M., Heine, A., Chen, Y., Luna, E. P., Todaro, T., Zhang, Y., Williams, P. A., McRee, D. E., Hirst, J., Stout, C. D., and Fee, J. A. (2003) High Resolution Structure of the Soluble, Respiratory-Type Rieske Protein from *Thermus thermophilus*: Analysis and Comparison. *Biochemistry 42*, 7303–7317.
21. Fee, J. A., Findling, K. L., Yoshida, T., Hille, R., Tarr, G. E., Hearshen, D. O., Dunham, W. R., Day, E. P., Kent, T. A., and Münck, E. (1984) Purification and Characterization of the Rieske Iron-Sulfur Protein from *Thermus thermophilus*. *J. Biol. Chem. 259*, 124–133.
22. Kuila, D., and Fee, J. A. (1986) Evidence for a Redox-Linked Ionizable Group Associated with the [2Fe-2S] Cluster of the *Thermus* Rieske Protein. *J. Biol. Chem. 261*, 2768–2771.
23. Link, T. A. (1994) Two pK_a Values of the Oxidised "Rieske" [2Fe-2S] Cluster Observed by CD Spectroscopy. *Biochim. Biophys. Acta 1185*, 81–84.
24. Gubernator, B. K. J., Kallas, T., and Szczepaniak, A. (2006) Iron-Sulfur Cluster Reconstitution of Spinach Chloroplast Rieske Protein

Requires a Partially Prefolded Apoprotein. *Biochim. Biophys. Acta 1764*, 735–742.
25. Link, T. A., Hatzfeld, O. M., Unalkat, P., Shergill, J. K., Cammack, R., and Mason, J. R. (1996) Comparison of the "Rieske" [2Fe-2S] Center in the bc_1 Complex and in Bacterial Dioxygenases by Circular Dichroism Spectroscopy and Cyclic Voltammetry. *Biochemistry 35*, 7546–7552.
26. Couture, M. M., Colbert, C. L., Babini, E., Rosell, F. I., Mauk, A. G., Bolin, J. T., and Eltis, L. D. (2001) Characterization of BphF, a Rieske-Type Ferredoxin with a Low Reduction Potential. *Biochemsitry 40*, 84–92.
27. Lindman, S., Linse, A., Mulder, F. A. A., and Andre, I. (2007) pK_a Values for Side-Chain Carboxyl Groups of a PGB1 Variant Explain Salt and pH-Dependent Stability. *Biophys. J. 92*, 257–266.
28. Hope, H. (1988) Crystallography of Biological Macromolecules: A Generally Applicable Method. *Acta Crystallogr., B B44*, 22–26.
29. Otwinowski, Z., and Minor, W. (2001) International Tables for Crystallography , pp 226−235, Kluwer, Dordecht, The Netherlands.
30. Vagin, A., and Teplyakov, A. (1997) Molrep: An Automated Program for Molecular Replacement. *J. Appl. Crystallogr. 30*, 1022–1025.
31. Murshudov, G. N., Vagin, A. A., and Dodson, E. (1997) Refinement of Macromolecular Structures by the Maximum-Likelihood Method. *Acta Crystallogr., D D53*, 240–255.
32. McRee, D. E. (1999) XtalView/Xfit—A Versatile Protein for Manipulating Atomic Coordinates and Electron Density. *J. Struct. Biol. 125*, 156–165.
33. Zu, Y., Fee, J. A., and Hirst, J. (2002) Breaking and Re-Forming the Disulfide Bond at the High-Potential, Respiratory-Type Rieske [2Fe-2S] Center of *Thermus thermophilus*: Characterization of the Sulfhydryl State by Protein-Film Voltammetry. *Biochemistry 41*, 14054–14065.
34. Alder, A. J., Greenfield, N. J., and Fasman, G. D. (1973) Circular Dichroism and Optical Rotary Dispersion of Proteins and Polypeptides. *Methods Enzymol. 27*, 675–735.
35. Pettersen, E. F., Goddard, T. D., Huang, C. C., Couch, G. S., Greenblatt, D. M., Meng, E. C., and Ferrin, T. E. (2004) UCSF Chimera—A Visualization System for Exploratory Research and Analysis. *J. Comput. Chem. 25*, 1605–1612.
36. Iwata, S., Saynovits, M., Link, T. A., and Michel, H. (1996) Structure of a Water Soluble Fragment of the "Rieske" Iron-Sulfur Protein of the Bovine Heart Mitochondrial Cytochrome bc_1 Complex Determined by MAD Phasing at 1.5 Å Resolution. *Structure 4*, 567–579.
37. Carrell, C. J., Zhang, H., Cramer, W. A., and Smith, J. L. (1997) Biological Identity and Diversity in Photosynthesis and Respiration: Structure of the Lumen-Side Domain of the Chloroplast Rieske Protein. *Structure 5*, 1613–1625.
38. Johnson, C. R., Shepherd, R. E., Marr, B., O'Donnell, S., and Dressick, W. (1980) Affinities of Imidazolate and Imidazole Ligands for Pentacyanoiron(III). *J. Am. Chem. Soc. 102*, 6227–6235.
39. McMillin, D. R. (2000) Electronic Absorption Spectroscopy, in Physical Methods in Bioinorganic Chemistry: Spectroscopy and Magnetism (Que, L., Ed.) pp 19−20, University Science Books, Sausalito, CA.
40. Johnson, M. K. (2000) CD and MCD Spectroscopy, in Physical Methods in Bioinorganic Chemistry (Que, L., Ed.) pp 233−285, University Science Books, Sausalito, CA.
41. Lange, C., and Hunte, C. (2002) Crystal Structure of the Yeast Cytochrome bc_1 Complex with its Bound Substrate Cytochrome *c*. *Proc. Natl. Acad. Sci. U.S.A. 99*, 2800–2805.
42. Gurung, B., Yu, L., and Yu, C. A. (2008) Stigmatellin Induces Reduction of Iron-Sulfur Protein in the Oxidized Cytochrome bc_1 Complex. *J. Biol. Chem. 283*, 28087–28094.
43. Crowley, P. J., Berry, E. A., Cromartie, T., Daldal, F., Godfrey, C. R., Lee, D. W., Phillips, J. E., Taylor, A., and Viner, R. (2008) The Role of Molecular Modeling in the Design of Analogues of the Fungicidal Natural Products Crocacins A and D. *Bioorg. Med. Chem. 16*, 10345–10355.
44. Kolling, D. J., Brunzelle, J. S., Lhee, S., Crofts, A. R., and Nair, S. K. (2007) Atomic Resolution Structures of Rieske Iron-Sulfur Protein: Role of Hydrogen Bonds in Tuning the Redox Potential of Iron-Sulfur Clusters. *Structure 15*, 29–38.
45. Kounosu, A., Li, Z., Cosper, N. J., Sokes, J. E., Scott, R. A., Iai, T., Urushiyama, A., and Iwasaki, T. (2004) Engineering a Three-Cysteine, One-Histidine Ligand Environment into a Hyperthermophilic Archeal Rieske-Type Ferredoxin from *Sulfolobus solfataricus*. *J. Biol. Chem. 279*, 12519–12528.
46. Lin, I., Chen, Y., Fee, J. A., Song, J., Westler, W. M., and Markley, J. L. (2006) Rieske Protein from *Thermus thermophilus*: ^{15}N NMR Titration Study Demonstrates the Role of Iron-Ligated Histidines in the pH Dependence of the Reduction Potential. *J. Am. Chem. Soc. 128*, 10672–10673.
47. Kuila, D., Schoonover, J. R., Dyer, R. B., Batie, C. J., Ballou, D. P., Fee, J. A., and Woodruff, W. H. (1992) Resonance Raman Studies of Rieske-Type Proteins. *Biochim. Biophys. Acta 1140*, 175–183.
48. Iwaki, M., Yakovlev, G., Hirst, J., Osyczka, A., Dutton, P. L., Marshall, D., and Rich, P. R. (2005) Direct Observation of Redox-Linked Histidine Protonation Changes in the Iron-Sulfur Protein of the Cytochrome bc_1 Complex by ATR-FTIR Spectroscopy. *Biochemistry 44*, 4230–4237.
49. Ullmann, G. M., Noodleman, L., and Case, D. A. (2002) Density Functional Calculation of pK_a Values and Redox Potentials in the Bovine Rieske Iron-Sulfur Protein. *J. Biol. Inorg. Chem. 7*, 632–639.
50. Walba, H., and Insensee, R. W. (1956) Spectrophotometric Study of the Acid Strength of Imidazole. *J. Org. Chem. 21*, 702–704.
51. George, P., Hanania, G. I. H., Irvine, D. H., and Asu-Issa, I. (1964) Effect of Coordination on Ionization. Part IV. Imidazole and it Ferrimyoglonin Complex. *J. Chem. Soc.,* 5679–5683.
52. Sievers, G., Gadsby, P. M. A., Peterson, J., and Thomson, A. J. (1983) Magnetic Circular Dichroism Spectra of Soybean Leghemoglobin *a* at Room Temperature and 4.2 K. *Biochim. Biophys. Acta 742*, 637–647.